ISSN 1061-8309, Russian Journal of Nondestructive Testing, 2017, Vol. 53, No. 10, pp. 731–743. © Pleiades Publishing, Ltd., 2017.

RADIATON METHODS

The Performance of Some Implicit Region-Based Active Contours in Segmenting and Restoring Welding Radiographic Images[1]

Y. Boutiche[a, b, *] and M. Halimi[a, **]

[a] *Research Center in Industrial Technologies CRTI, ex CSC, Image and Signal Processing Laboratory, Algiers, 16014 Algeria*

[b] *Département d'Électronique, Faculté de Technologie, Université Saâd Dahlab de Blida, Blida, 09000 Algérie*

**e-mail: y.boutiche@crti.dz; bouticheyami@gmail.com*

***e-mail: halimi_md@yahoo.fr*

Received June 28, 2016; in final form, January 17, 2017

Abstract—Several domains are based on image processing and analysis. One of them is the radiographic inspection which is used in Non Destructive Testing (NDT). Active contours, snakes or deformable models are powerful techniques in image segmentation and restoration. According to the term related to the input data (image to be treated) those functionals are ranked on two categories: edge-based models and region-based models. Previous studies point out the advantages of the region-based models over edge-based models. In this paper, we discuss and we summarize the strengths and weaknesses of four implicit region-based active contour models named: Piecewise Constant PC, Piecewise Smooth PS, Local Binary Fitting LBF and Global Local fitting energy GLF. After performing several experiments, we have concluded that all the models perform well with homogeneous images. On the contrary when images are strongly inhomogeneous, the models based on global (PC) or local (LBF) statistic intensity fail to segment such images. The PS model with its great advantage in preserving the contours has, as a drawback, the high CPU time consuming. The combination of local and global statistic image intensity gives to the GLF model the ability to better deal with such images in less CPU time.

DOI: 10.1134/S1061830917100035

1. INTRODUCTION

Nowadays the visual information has being introduced in very large applications. The image processing field becomes more and more important. The primordial task in image analysis is the segmentation. Segmentation and restoration via active contours or deformable models have known greater use in different domains. We distinguish, essentially, two classes of active contours (deformable models): edge-based models [1–6] and region-based models [7–13]. We focus on models which are based on region due to their advantages over the once based on contour. They do not use image gradient, are less sensitive to noise, can successfully segment objects with weak edges or without edge, interior contours can be automatically detected, and they are less sensitive to initial contour location.

In this context, the older and famous functional is the Mumford–Shah model [14], this one has limit applications due to its high complexity. Later, several functional (weak formulation) had been proposed. Generally speaking, all region-based models could be ranged in three classes as follows: Global region-based models, Local region-based models, and Global Local (hybrid) region-based models. In the Global region-based models category, we cite the one called piecewise constant approximation PC, proposed by Chan and Vese [7], where the resulting image u is approximated by a set of constants. This model has known great success in segmenting homogenous images especially when it was improved by introducing multiphase level set. Even though, this model fails within inhomogeneous intensity distribution which is the case for large real images. To overcome these limitations, the same authors proposed the piecewise smooth approximation PS model where u is approximated by set of functions of C^1 class [11]. Such

[1] The article is published in the original.

approximation allows the PS model to deal with inhomogeneous images. Generally, models based on global statistic information ignored totally the intensity variation inside regions. Such works have been followed by others models that are based on local statistic information, this local property is, more often, assured by the Gaussian kernel function [15–19]. More recently, some papers have proposed an hybrid functional, where the contour in evolution is attracted to the objects' boundaries via a combination between global and local statistic image information [20, 21].

The rest of the paper is structured as follows: Section 2 is devoted to present the region-based models. In Section 3, we detail and exhibit the outcomes of these models on radiographic images to show their performance on segmentation and restoration; furthermore discussions on some influencing parameters are presented. We end this paper with a conclusion and by giving some suggestions on the radiographic image segmentation.

2. SOME REGION-BASED DEFORMABLE MODELS

This section is devoted to look over through the recent literature which is based on using image region information to drive the curve in evolution through the objects' boundaries. The very interesting property of these models is that they solve two common image-processing tasks simultaneously: image denoising or restoration and image segmentation. For the rest of the paper, we denote by $\Omega \in \mathcal{R}^N$ a bound domain and u_0: $\Omega \to \mathcal{R}$ represents a grayscale image.

2.1. Mumford-Shah Model

The oldest and popular model in image region based segmentation is the one proposed by Mumford and Shah [14]. Authors had formulated a functional capable to divide the image domain into non overlapping regions separated by contours C representing various limits of objects. Consequently, the following energy was proposed:

$$E^{\mathrm{MS}}(u,C) = \int_{\Omega} (u-u_0)^2\,dx + \mu \int_{\Omega/C} |\nabla u|^2\,dx + \nu|C|, \tag{1}$$

where $\mu, \nu > 0$ are constants to penalize the different terms, u is the optimal approximation of the original image u_0, Ω is the image domain. The signification of the three terms in the functional is as follows: the first integral represents fidelity to data, its minimization approximates the u to u_0. The second integral is the smoothing term which makes u smooth inside each region but not at the boundaries, and the last term regularizes the contour. However, the minimization of $F^{\mathrm{MS}}(u, C)$ gives an image u with minimum complexity (cartoon image) and objects' boundaries. In practice, it is so difficult to solve Eq. (1) due to two serious problems: the different dimensions of C and u, and the non convexity of $F^{\mathrm{MS}}(u, C)$ which can provide multiple local minima.

2.2. Piecewise Constant Approximation PC

The PC model was proposed by Chan and Vese [7] to overcome the difficulties in solving Eq. (1). The first *PC* model is based on simplifying Mumford–Shah functional by approximating the image u to set of constants (two constants). The functional to be minimized is given by Eq. (2):

$$E^{\mathrm{PC}}(c_{\mathrm{in}}, c_{\mathrm{out}}, C) = \lambda_1 \int_{\mathrm{inside}(C)} (u_0 - c_{\mathrm{in}})^2\,dx + \lambda_2 \int_{\mathrm{out}(C)} (u_0 - c_{\mathrm{out}})^2\,dx + \nu|C|, \tag{2}$$

where $\nu > 0$, $\lambda_1, \lambda_2 > 0$; c_{in} and c_{out} are, respectively, the average image intensity inside and outside curve. The Eq. (2) can be written via an implicit representation of the curve using level set function Φ introduced by Osher [22] as follows:

$$\begin{aligned} E^{\mathrm{PC}}(c_{\mathrm{in}}, c_{\mathrm{out}}, \Phi) = \lambda_1 \int_{\Omega} (u_0 - c_{\mathrm{in}})^2 H_\epsilon(\Phi(x))\,dx + \lambda_2 \int_{\Omega} (u_0 - c_{\mathrm{out}})^2 (1 - H_\epsilon(\Phi(x)))\,dx \\ + \nu \int_{\Omega} |\nabla H_\epsilon(\Phi(x))|\,dx. \end{aligned} \tag{3}$$

The according Euler–Lagrange equation that allows the evolution of the curve is given by the following Eq. (4)

$$\frac{\partial \Phi}{\partial t} = \delta_\epsilon(\Phi)\left[\nu \operatorname{div}\frac{\nabla\Phi}{|\nabla\Phi|} - \lambda_1(u_0 - c_{\text{in}})^2 + \lambda_2(u_0 - c_{\text{out}})^2\right]. \tag{4}$$

When the minimization of the functional is reached, the restored image can be represented by the following formulation:

$$u^{\text{PC}}(x) = c_{\text{in}} H_\epsilon(\Phi(x)) + c_{\text{out}}(1 - H_\epsilon(\Phi(x))),$$

where Φ is the level set function, $H_\epsilon(\Phi)$ is the regularized version of Heaviside function, used to identify the inside and outside regions. It is formulated by Eq. (5) and its derivative $\delta_\epsilon(\Phi)$ by Eq. (6).

$$H_\epsilon(x) = \frac{1}{2}\left[1 + \frac{2}{\pi}\arctan\left(\frac{z}{\epsilon}\right)\right], \tag{5}$$

$$\delta_\epsilon(x) = \frac{1}{\pi}\frac{\epsilon}{\epsilon^2 + z^2}; \quad z \in R. \tag{6}$$

The model has great success due to its multiple advantages such as its less sensitivity to initial condition, its capacity to extract blurred boundaries and its ability to segment noisy images. Nevertheless, those successful results are getting within images with homogenous intensity distributions, but the model fails when the image intensities are inhomogeneous, this is explained by the fact that PC model compute the global average intensity inside and outside the curve in evolution which can be far different from the original image. The authors have improved their model by introducing multiphase level set [11] on which u is approximated by more than two constants. Despite this, solving the problem of inhomogeneous images remains to be determined.

2.3. Piecewise Smooth Approximation PS

In the aim to treat largest modalities of images, Chan and Vese proposed functional that approximate u by two piecewise smooth functions u^+ and u^- [11]. The weak form of the Mumford-Shah functional with such approximation of u, and via an implicit representation of the curve C is given by the Eq. (7).

$$\begin{aligned} F(u^+, u^-, \Phi) &= \int_\Omega |u^+ - u_0|^2 H_\epsilon(\Phi(x))\,dx \\ &+ \int_\Omega |u^- - u_0|^2 (1 - H_\epsilon(\Phi(x)))\,dx + \mu\int_\Omega |\nabla u^+|^2 H_\epsilon(\Phi(x))\,dx \\ &+ \mu\int_\Omega |\nabla u^-|^2 (1 - H_\epsilon(\Phi(x)))\,dx + \nu\int_\Omega |\nabla H_\epsilon(\Phi(x))|\,dx, \end{aligned} \tag{7}$$

where u^+ and u^- are two functions of C^1 class that approximate smoothly the inside and outside of the curve. To minimize the functional (7), we firstly, fix Φ to get the Euler–Lagrange equations of u^+ and u^-.

$$\begin{aligned} u^+ - u_0 &= \mu\Delta u^+ \quad \text{in} \quad x \in \Omega : \Phi(x,t) > 0; \\ \frac{u^+}{\partial \vec{n}} &= 0 \quad \text{on} \quad x \in \Omega : \Phi(x,t) = 0, \end{aligned} \tag{8}$$

$$\begin{aligned} u^- - u_0 &= \mu\Delta u^- \quad \text{in} \quad x \in \Omega : \Phi(x,t) < 0; \\ \frac{u^-}{\partial \vec{n}} &= 0 \quad \text{on} \quad x \in \Omega : \Phi(x,t) = 0. \end{aligned} \tag{9}$$

Now for u^+ and u^- fixed, we obtain the Euler–Lagrange Eq. (10) that allows the evolution of curve (Level set).

$$\frac{\partial \Phi}{\partial t} = \delta_\epsilon \Phi\left[\mu \operatorname{div}\left(\frac{\nabla\Phi}{|\nabla\Phi|}\right) - |u^+ - u_0|^2 - \mu|\nabla u^+|^2 + |u^- - u_0|^2 + \mu|\nabla u^-|^2\right]. \tag{10}$$

The restored image is the combination between the two smooth functions as follows:

$$u^{\mathrm{PS}}(x) = u^{+}(x) H_{\epsilon}(\Phi(x)) + u^{-}(x)(1 - H_{\epsilon}(\Phi(x))).$$

The PS model has limited applications in practice, due to its algorithm complexity and time consuming [20]: we have to solve at least, in each iteration, five partial differential equations: Two equation to get u^{+} and u^{-}, followed by another two PDE equations to extend u^{+} to $\Phi < 0$ and u^{-} to $\Phi \geq 0$. Such tasks are difficult to implement and increase strongly the computational cost. The fifth PDE (Eq. (10)) is to update the level set function. In addition a re-initialization step is often suggested to maintain the stability of the evolution.

2.4. Local Binary Fitting Model LBF

Region-based segmentation has been efficiently improved by introducing the LBF model. C. Li et al. [17] proposed a model based on approximating locally the image intensities inside and outside curve. The energy functional is defined as follows:

$$\begin{aligned} E^{\mathrm{LBF}}(C, f_1, f_2) = \lambda_1 \int\limits_{\mathrm{in}(C)} K_{\sigma}(x-y)\left|u_0(y) - f_1(x)\right|^2 dy \\ + \lambda_2 \int\limits_{\mathrm{out}(C)} K_{\sigma}(x-y)\left|u_0(y) - f_2(x)\right|^2 dy, \end{aligned} \tag{11}$$

where x and y are points of image, σ, λ_1, and λ_2 are positive constants, K_{σ} is a Gaussian kernel which is a weighting function with a localization property. $f_1(x)$ and $f_2(x)$ are the two numbers that fit image intensities near the centre point x. As it is known the Gaussian kernel $K_{\sigma}(x-y)$ takes large values at the points y near the center point x, and radically decreases to 0 as y goes away from x($K_{\sigma}(x-y) \to 0$ when $|x-y| \to \infty$). However, the value of $f_1(x)$ and $f_2(x)$ for each point x are dominated by the image intensities near the centre point x. The functional $E^{\mathrm{LBF}}(C, f_1, f_2)$ in Eq. (11) is rewritten via level set function as:

$$\begin{aligned} E^{\mathrm{LBF}}(f_1, f_2, \Phi) = \lambda_1 \int \left[\int K_{\sigma}(x-y)\left|u_0(y) - f_1(x)\right|^2 H(\Phi(y))\, dy\right] dx \\ + \lambda_2 \int \left[\int K_{\sigma}(x-y)\left|u_0(y) - f_2(x)\right|^2 (1 - H(\Phi(y)))\, dy\right] dx. \end{aligned} \tag{12}$$

The functional in Eq. (12) needs to be improved in order to ensure stable evolution of level set function. For that, and inspired from the work published by Li et al. [5], the authors add the distance regularizing term to penalize the deviation of the level set function from a signed function. This term is characterized by the following integral:

$$D(\Phi) = \int\limits_{\Omega} \frac{1}{2}\left(\left|\nabla\Phi(x)\right| - 1\right)^2 dx. \tag{13}$$

Another term is necessary to regularize the zero level set contour. This one is formulated as follows:

$$L(\Phi) = \int\limits_{\Omega} \delta_{\epsilon}(\Phi(x))\left|\nabla\Phi(x)\right| dx. \tag{14}$$

The final functional of LBF model to be minimized is the addition of the three integrals

$$F^{\mathrm{LBF}}(f_1, f_2, \Phi) = E^{\mathrm{LBF}}(f_1, f_2, \Phi) + \beta D(\Phi) + \nu L(\Phi). \tag{15}$$

Based on calculus of variation [23] we get the Euler-Lagrange equations that minimized $F^{\mathrm{LBF}}(f_1, f_2, \Phi)$. For fixed level set Φ the $f_1(x)$ and $f_2(x)$ that minimize (15) satisfy the following equations:

$$\int K_{\sigma}(x-y) H_{\epsilon}(\Phi(y))(u_0(y) - f_1(x))dy = 0,$$

$$\int K_{\sigma}(x-y)(1 - H_{\epsilon}(\Phi(y)))(u_0(y) - f_2(x))dy = 0.$$

By development and putting out the term independent from integral, we get the formulation of $f_1(x)$ and $f_2(x)$

$$f_1(x) = \frac{K_{\sigma}(x) * [H_{\epsilon}(\Phi(x)) u_0(x)]}{K_{\sigma}(x) * [H_{\epsilon}(\Phi(x))]}, \tag{16}$$

$$f_2(x) = \frac{K_\sigma(x) * [(1 - H_\epsilon(\Phi(x)))u_0(x)]}{K_\sigma(x) * [1 - H_\epsilon(\Phi(x))]}. \tag{17}$$

Now we keep $f_1(x)$ and $f_2(x)$ fixed and we compute the Euler–Lagrange equation that allows the update of level set function

$$\begin{aligned}\frac{\partial\Phi}{\partial t} = -\delta_\epsilon(\Phi)(\lambda_1 e_1 - \lambda_2 e_2) + \nu\delta_\epsilon\Phi\,\mathrm{div}\left(\frac{\nabla\Phi}{|\nabla\Phi|}\right)\\ + \beta\left(\nabla^2\Phi - \mathrm{div}\left(\frac{\nabla\Phi}{|\nabla\Phi|}\right)\right),\end{aligned} \tag{18}$$

where e_1 and e_2 are given by:

$$\begin{aligned}e_1(x) &= \int_\Omega K_\sigma(y-x)|u_0(x) - f_1(y)|^2\,dy,\\ e_2(x) &= \int_\sigma K_\sigma(y-x)|u_0(x) - f_2(y)|^2\,dy.\end{aligned}$$

These two equations should be developed to get:

$$\begin{aligned}e_1(x) = u_0^2(x)[1 * K_\sigma(x)]\\ - 2u_0(x)[f_1(x) * K_\sigma(x)] + f_1^2(x) * K_\sigma(x),\end{aligned} \tag{19}$$

$$\begin{aligned}e_2(x) = u_0^2(x)[1 * K_\sigma(x)]\\ - 2u_0(x)[f_2(x) * K_\sigma(x)] + f_2^2(x) * K_\sigma(x).\end{aligned} \tag{20}$$

Similarly to the above models, the restored image via the LBF model is given by:

$$u^{\mathrm{LBF}}(x) = f_1(x)H_\epsilon(\Phi(x)) + f_2(x)(1 - H_\epsilon(\Phi(x))).$$

2.5. Global and Local Gaussian Distribution Fitting Model GLF

The above discussed models are based on global fitting term or local one. Recently Wang et al. [21] have proposed an hybrid model, where the fidelity term in the functional to be minimized is a combination between global and local statistical image information. They have proposed the following functional:

$$\begin{aligned}E^{\mathrm{GLF}}\left(\Phi, u_1(x), u_2(x), \sigma_1^2(x), \sigma_2^2(x), u_3, u_4, \sigma_3^2, \sigma_4^2\right)\\ = E^R(\Phi) + (1-\theta)E^L\left(\Phi, u_1(x), u_2(x), \sigma_1^2(x), \sigma_2^2(x) + \theta E^G\left(u_3, u_4, \sigma_3^2, \sigma_4^2\right)\right),\end{aligned} \tag{21}$$

where E^R represents the regularization term, E^L the local term and E^G the global term. They are formulated as follows:

$$E^R(\Phi) = \nu\int|\nabla H(\Phi(x))|, \tag{22}$$

$$\begin{aligned}E^L\left(\Phi, u_1(x), u_2(x), \sigma_1^2(x), \sigma_2^2(x)\right)\\ = \int\left[\int K_\sigma(x-y)\left(\log\sqrt{2\pi} + \log\sigma_1(x) + \frac{(u_0(y) - u_1(x))^2}{2\sigma_1^2(x)}\right)H_\epsilon(\Phi(x))\,dy\right]dx\\ + \int\left[\int K_\sigma(x-y)\left(\log\sqrt{2\pi} + \log\sigma_2(x) + \frac{(u_0(y) - u_2(x))^2}{2\sigma_2^2(x)}\right)(1 - H_\epsilon(\Phi(y)))\,dy\right]dx,\end{aligned} \tag{23}$$

$$E^{G}\left(u_3,u_4,\sigma_3^2,\sigma_4^2\right)$$
$$=\int\left(\log\sqrt{2\pi}+\log\sigma_3+\frac{\left(u_0(x)-u_3\right)^2}{2\sigma_3^2}\right)H_\epsilon\left(\Phi(x)\right)dx \tag{24}$$
$$+\int\left(\log\sqrt{2\pi}+\log\sigma_4+\frac{\left(u_0(x)-u_4\right)^2}{2\sigma_4^2}\right)\left(1-H_\epsilon\left(\Phi(x)\right)\right)dx.$$

The indexes $i = 1, 2$ is used to identify the local statistical image informations, and $j = 3, 4$ is used for the global ones. An additional term is necessary for maintaining the signed distance property of level set during evolution, such term allows regular and stable LS evolution without the need to re-initialization step.

$$R_p(\Phi)=\int p\left(\left|\nabla\Phi(x)\right|\right)dx, \tag{25}$$

where p is the double-well potential function given by:

$$p(z)=\begin{cases}\dfrac{1}{(2\pi)^2}\left(1-\cos(2\pi z)\right), & \text{if } z>1,\\ \dfrac{1}{2}(z-1)^2, & \text{if } z\geq 1 \quad z\in R.\end{cases} \tag{26}$$

By the introduction of the regular version of Heaviside function (Eq. (5)), the whole functional of LGF model is expressed as follows:

$$F^{\mathrm{GLF}}\left(\Phi,u_1(x),u_2(x),\sigma_1^2(x),\sigma_2^2(x),u_3,u_4,\sigma_3^2,\sigma_4^2\right)$$
$$=E^{\mathrm{GLF}}\left(\Phi,u_1(x),u_2(x),\sigma_1^2(x),\sigma_2^2(x),u_3,u_4,\sigma_3^2,\sigma_4^2\right)+\mu R_p(\Phi), \tag{27}$$

where $\mu > 0$.

As almost all deformable models (active contours) the minimization of the functional is ensured by the gradient descent method, where in order to find each variable we fix the others then we use the calculus of variations principle to get its equation. Then we obtain the local and global means and variances as follows:

$$u_1(x)=\frac{\int K_\sigma(x-y)\,u_0(y)\,H_\epsilon\left(\Phi(y)\right)dy}{\int K_\sigma(x-y)\,H_\epsilon\left(\Phi(y)\right)dy}, \tag{28}$$

$$u_2(x)=\frac{\int K_\sigma(x-y)\,u_0(y)\left(1-H_\epsilon\left(\Phi(y)\right)\right)dy}{\int K_\sigma(x-y)\left(1-H_\epsilon\left(\Phi(y)\right)\right)dy}, \tag{29}$$

$$\sigma_1^2(x)=\frac{\int K_\sigma(x-y)\left(u_0(y)-u_1(x)\right)^2H_\epsilon\left(\Phi(y)\right)dy}{\int K_\sigma(x-y)\,H_\epsilon\left(\Phi(y)\right)dy}, \tag{30}$$

$$\sigma_2^2(x)=\frac{\int K_\sigma(x-y)\left(u_0(y)-u_2(x)\right)^2\left(1-H_\epsilon\left(\Phi(y)\right)\right)dy}{\int K_\sigma(x-y)\left(1-H_\epsilon\left(\Phi(y)\right)\right)dy}, \tag{31}$$

$$u_3=\frac{\int u_0(x)\,H_\epsilon\left(\Phi(x)\right)dx}{\int H_\epsilon\left(\Phi(x)\right)dx}, \tag{32}$$

$$u_4=\frac{\int u_0(x)\left(1-H_\epsilon\left(\Phi(x)\right)\right)dx}{\int\left(1-H_\epsilon\left(\Phi(x)\right)\right)dx}, \tag{33}$$

$$\sigma_3^2 = \frac{\int (u_0(x) - u_3)^2 H_\epsilon(\Phi(x))dx}{\int H_\epsilon(\Phi(x))dx}, \tag{34}$$

$$\sigma_4^2 = \frac{\int (u_0(x) - u_4)^2 (1 - H_\epsilon(\Phi(x)))dx}{\int (1 - H_\epsilon(\Phi(x)))dx}. \tag{35}$$

Minimizing the functional (27) with respect to Φ (keep all variables fixed except Φ); we get the updating equation as follows:

$$\begin{aligned}\frac{\partial \Phi}{\partial t} = \mu \operatorname{div}(d_p(|\nabla\Phi|)\nabla\Phi) + \nu\delta_\epsilon(\Phi)\operatorname{div}\left(\frac{\nabla\Phi}{|\nabla\Phi|}\right) \\ - \delta_\epsilon(\Phi)[(1-\theta)(e_1 - e_2) + \theta(e_3 - e_4)],\end{aligned} \tag{36}$$

where

$$d_p(z) = \frac{p'(z)}{z},$$

e_1 and e_2 are the local terms, they are given by:

$$e_i = \int K_\sigma(y - x)\left(\log\sigma_i(y) + \frac{(u_0(x) - u_i(y))^2}{2\sigma_i^2(y)}\right)dy, \quad i = 1,2. \tag{37}$$

The global terms e_3 and e_4 are formulated as follows:

$$e_j = \log\sigma_j + \frac{(u_0(x) - u_j)^2}{2\sigma_j^2}, \qquad j = 3,4. \tag{38}$$

Note that $u_1(x)$ and $u_2(x)$ (Eqs. (28) and (29)) are identical to $f_1(x)$ and $f_2(x)$ in Eqs. (16) and (17). In addition, the global terms u_3 and u_4 are equivalent to c_{in} and c_{out} in the PC model. Such combination has improved the performance on segmentation and speed up the convergence. Furthermore, the constant θ, $(0 \le \theta \le 1)$ is a coefficient which adjusts the ratio between the local and global region fitting energies. In the case of GLF model the restored image is

$$\begin{aligned}u^{GLF}(x) = [(1-\theta)u_1(x) + \theta u_3]H(\Phi(x)) \\ + [(1-\theta)u_2(x) + \theta u_4](1 - H(\Phi(x))).\end{aligned}$$

3. WELD RADIOGRAPHIC SEGMENTATION AND RESTORATION

The interpretation of radiographs takes place in three basic steps: detection, interpretation and evaluation. The automatization of such tasks is based on image processing and analysis. Our team works on weld radiographic images segmentation and restoration, in order to use them for radiographic inspection. More often, such kind of images, have low contrast and inhomogeneous grayscale distribution. More details about the x-rays image used in this work can be found in [24].

In this section, we are going to apply the four models discussed previously on some different x-ray images to see the behaviour and performance of these models in restoring, extracting the boundaries of weld joints and/or weld defects. We have implemented the four models via an implicit representation of the contour using *Level Set Function* (LSF). For PC and PS models a *Signed Distance Function* SDF was used (Fig. 1b). For LBF and GLF models we used a Binary Function BF (Fig. 1c). The implicit representation has many advantages over the explicit one. It is able to handle sharp corners and cusps in the propagating solution, as well as topological changes. In addition it is defined in the grid image which ensure the continuity of the extracted contours. In our context, the weld features calculated from the results of segmentation will have an accuracy of a pixel.

Note that the space steps $h = \Delta x = \Delta y = 1$. We fix for all experiments $\lambda_1 = \lambda_2 = 1$, $\varepsilon = h$. The time step $\Delta t = 0.1$ for PC, LBF and GLF models and $\Delta t = 3$ for PS model. The parameter $\nu = \alpha \times 255^2$ where α depends on the processed image as well as μ, σ, and θ.

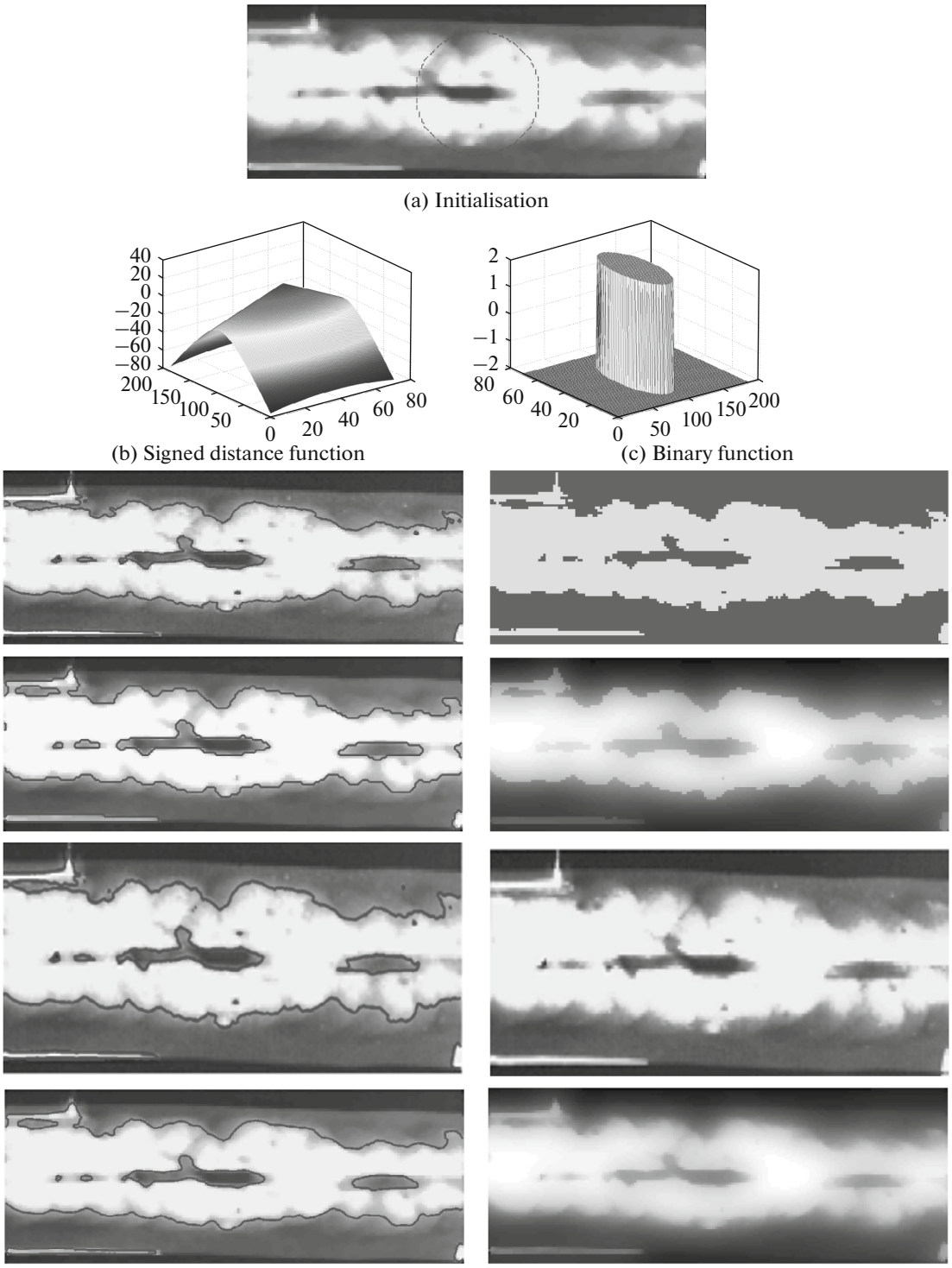

Fig. 1. Extracted contours (first column) and restoration (second column) of radiographic image with weak inhomogeneous intensity: First row PC model $\alpha = 0.004$. Second one LBF model with $\alpha = 0.001$, $\sigma = 6$, third one PS model with $\alpha = 0.030$, $\mu = 5$ and last row GLF model with $\alpha = 0.0046$, $\sigma = 6$ and $\theta = 0.5$.

The first experiment, shown in Fig. 1 concerns x-rays image of size [71 × 186], that presents low complexity and weak inhomogeneity. In this case the four models give similar segmentation results. In term of restoration the best restored image is the one obtained by PS model due to the high fidelity of the two functions u^+ and u^- to the processed image and the smoothing of regions without affecting objects' boundaries.

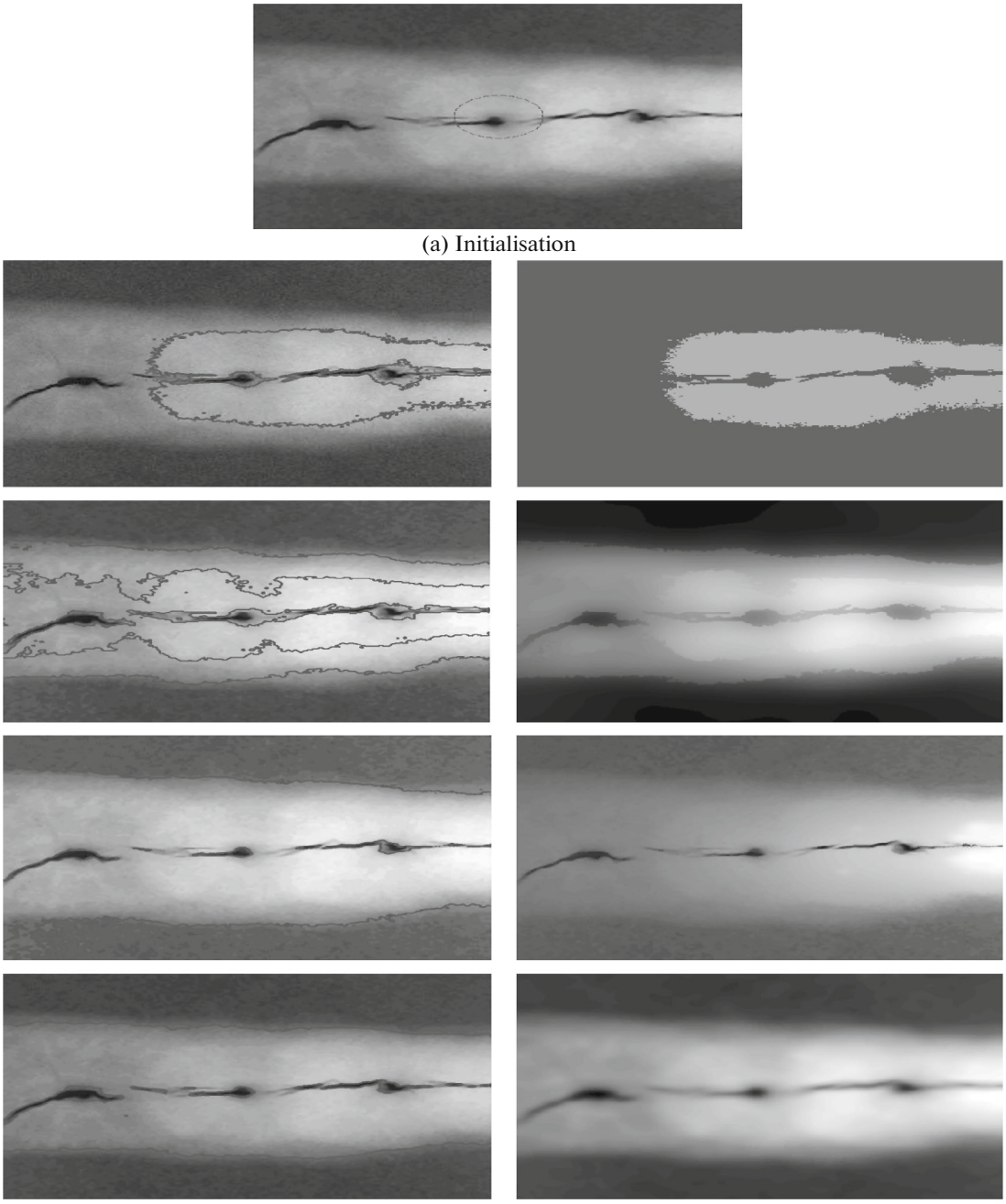

(a) Initialisation

Fig. 2. Extracted contours (first column) and restoration (second column) of radiographic image with strong inhomogeneous intensity: First row PC model $\alpha = 0.001$ Second one LBF model with $\alpha = 0.001$, $\sigma = 10$, third one PS model with $\alpha = 0.0045$, $\mu = 10$ and last row GLF model with $\alpha = 0.00016$, $\sigma = 3$, $\theta = 0.001$.

The second experiment is also an x-rays weld image of size [265 × 272] which presents strong inhomogeneity and more noise. The first row of Fig. 2 shows that PC model totally fails to segment this image. The LBF gives better results than the PC one. Its drawback resides in the strongly dependence on the value allocated to the Gaussian kernel size (σ). However, we have got different segmentation results for different values. On the contrary, the combination of global and local image information (GLF model) decreases considerably the influence of that parameter on the final results, where we have got the same segmentation results as the last row of Fig. 2 for large set of (from $\sigma = 3$ to $\sigma = 50$). The two last rows of Fig. 2 show that the PS and GLF models deal much better with such kind of images. Both models extract correctly all the well defects as well as the edges of weld joint. Note that the PS model provide more undesirable small

Table 1. The performance of the four models in terms of quality of restoration

		PC	LBF	PS	GLF
Exp. 1	MSE	1469.62	781.01	283.66	955.76
	PSNR(dB)	16.45	19.20	23.60	18.32
	UIQI	0.87	0.92	0.98	0.89
Exp. 2	MSE	1081	79.02	1045.76	38.29
	PSNR(dB)	17.79	29.15	17.93	32.29
	UIQI	0.70	0.98	0.73	0.99

Table 2. The performance of the four models in CPU time consuming (Processor: core(TM) i7-2600 CPU 3.40 GHZ, RAM: 4 Go)

		PC	LBF	PS	GLF
Exp. 1	Iterations	10	80	250	30
	CPU(s)	1.12	8.48	15.10	3.66
Exp. 2	Iterations	200	200	1750	50
	CPU(s)	7.60	50.84	700.16	5.97

contours even though we have increased the parameter of smoothing ($\mu = 10$). For the GLF we have set $\theta = 0.001$ in order to give more weight to the local term because of the nature of the image.

We introduce three metrics, often used, to evaluate the restoration algorithms [25]. The first one which is the Mean Squared Error MSE is given by:

$$\mathrm{MSE} = \frac{1}{nm}\sum_{i=0}^{m-1}\sum_{j=0}^{n-1}\left\|o(i,j) - r(i,j)\right\|^2. \tag{39}$$

The second one is the Peak Signal-to-Noise Ratio PSNR. It estimates the quality of reconstructed image compared with the original one.

$$\mathrm{PSNR} = 20\log_{10}\left(\frac{s}{\sqrt{\mathrm{MSE}}}\right), \tag{40}$$

where o and r represent the original and restored images respectively. $s = 255$ for an 8-bit images, $[m \times n]$ is the size of the image. The proposal is that the higher the PSNR, the better degraded image has been reconstructed to match the original image. The third metric is called Universal Image Quality Index UIQI which is based on three comparisons: luminance, contrast, and structural of the original and restored images [26] as follows:

$$l(o,r) = \frac{2\mu_0\mu_r}{\mu_0^2 + \mu_r^2}; \tag{41}$$

$$c(o,r) = \frac{2\sigma_0\sigma_r}{\sigma_0^2 + \sigma_r^2}; \tag{42}$$

$$s(o,r) = \frac{\sigma_o r}{\sigma_0\sigma_r}, \tag{43}$$

where μ_o and μ_r denote the mean values of the original and restored images respectively. The σ_o and σ_r are their standard deviation, and $\sigma_o r$ is the covariance of both images. The UIQI is calculated using the three above equations according to Eq. (44). The UIQI metric is ranged in the interval -1 (lowest value) and $+1$ (best value).

$$\mathrm{UIQI} = l(o,r)\times c(o,r)\times s(o,r) = \frac{4\mu_o\mu_r\sigma_o r}{\left(\mu_o^2 + \mu_r^2\right)\left(\sigma_o^2 + \sigma_r^2\right)}. \tag{44}$$

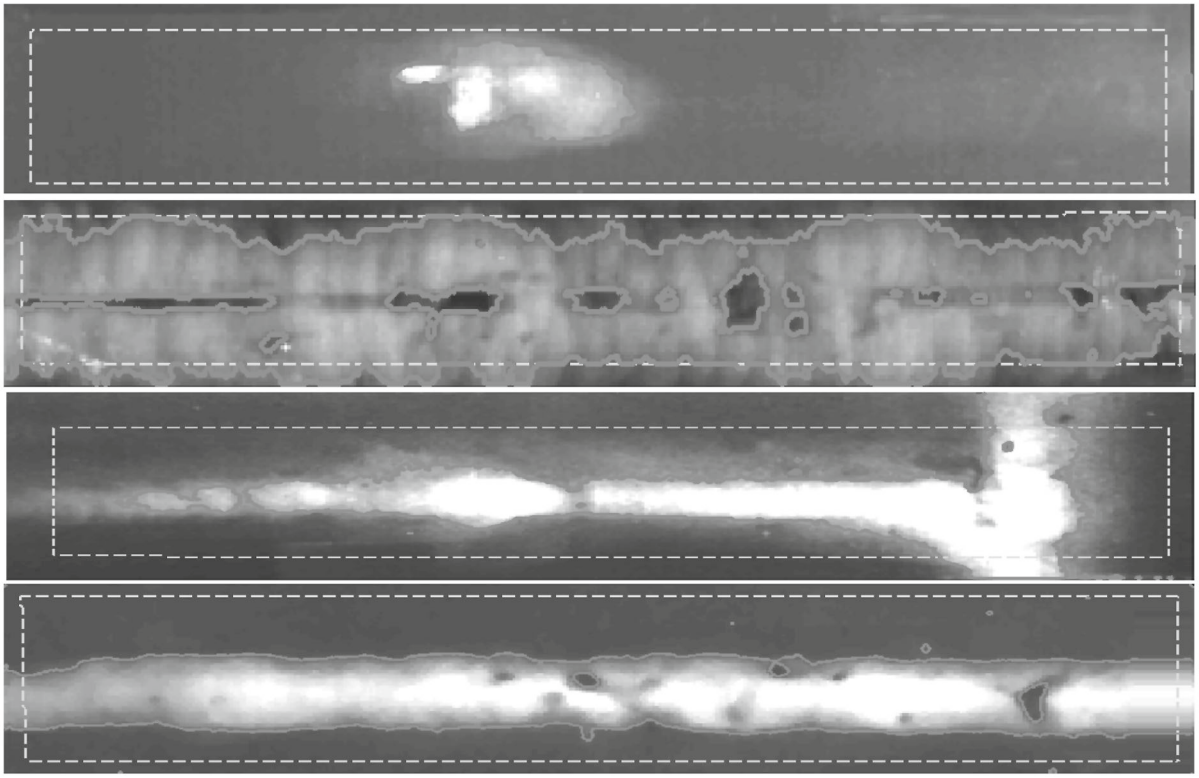

Fig. 3. Results on segmenting different kind of weld X-rays images by using GLF model.

In term of restoration and based on experiments displayed on the second column of Figs. 1 and 2, as well as the obtained results summarized in the Table 1, we can say that the restoration quality is comparable for the LBF, PS, GLF models. On the contrary, the PC model gives the worst results because the intensity variation inside the regions is totally ignored. Now we focus on the performance of the four models in term of algorithm complexity and therefore time consuming. Consequently, we have summarized the iteration numbers and CPU time necessary for the convergence for each model and for both experiments shown in Figs. 1 and 2.

More than the good results obtained via GLF model, Table 2 reveals clearly its power in term of convergence speed, where few iterations are enough to get the stationary state. Here we have to point out that the results obtained are related to the location of the contour initialization on the image domain. In practice, it is preferable to make an automatic initialization (as in our experiments in Fig. 3) for two reasons: reducing the user intervention and eliminating the dependence of results on initialization. Another parameter which is the temporal discretization step Δt influences the convergence speed. More often it is fixed to small value (0.001–0.5) to insure stable evolution; but it can be increased for the semi-implicit temporal discretization which is the case of the algorithm used to implement the PS model ($\Delta t = 3$).

On the Fig. 3 we display more outcomes of GLF on other welding x-rays images. We use dashed green line to present the contour initialization and the solid red line for final contour. We have chosen x-rays images for different welded alloys that present different kind of welding defects. The GLF model segment successfully the images by using the same parameters ($\alpha = 0.001$, $\theta = 0.0091$, $\sigma = 5$).

4. CONCLUSIONS

In this paper, a set of implicit region-based models for image segmentation and restoration has been summarized and discussed. Similar to active contours, they are based on a variational analysis and Partial Differential Equations. The differences between those models reside on the force that drives and attracts the active contour toward the objects' boundaries. However the optimal approximation of the original image u_0 is different.

PC model is based on a global statistic image information inside and outside curve. The advantage of PC model resides in its low algorithm complexity. It gives good results in homogenous image segmentation. The restoration with PC model consists just to label the foreground and background by two different constants. Such approximation ignores totally the intensity variations inside regions. However, PC model fails to segment inhomogeneous images which is the case of almost all real images.

On the contrary, the LBF model approximates the intensity locally by using a Gaussian kernel function, such approximation increases the ability of the model to deal with inhomogeneous images. In addition, the parameter σ has primordial influences in the final results, where small value makes model, on the one hand, very sensitive to intensity variation which provides on same region several subregions. On the second hand, the model will be very sensitive to initial contour location. On the contrary, large value of σ could merge two different regions. Consequently, in term of restoration, strong filtered band appear around extracted contours. LBF model deals better than PC model in the presence of weak inhomogeneous intensity variation; but it fails when the image is severely inhomogeneous.

The PS model, that approximates a given image by two functions of class C^1, takes into consideration also the slight intensity variation. With this approximation we get successful segmentation and restoration without any smoothing crossing the edges. The strong drawback of PS model is its highest algorithm complexity and time consuming, comparatively to other models.

The GLF model is an hybrid one; its functional is based on global and local statistic information (means and variances). This combination gives the GLF model many advantages: it deals very well with homogenous and inhomogeneous images, it is fast and less sensitive to initialization.

For industrial applications, a compromise between quality of treatments and execution time is needed. For that and in order to ensure a good first step processing chain (segmentation, restoration) of large set of radiographic images, we suggest to use the GLF. In the end we want to point out that even based-regions active contours have proved their great advantages in segmentation and restoration, some weaknesses present always challenging points for image processing community, such as: local minimum instead of global minimum (the non convexity of functionals), sensitivity to initial conditions (shape and location of initial contour), sensibility of the model to the set of parameters.

REFERENCES

1. Kass, M., Witkin, A., and Terzopoulos, D., Snakes: active contour models, *Int. J. Comput. Vision*, 1988, pp. 321–331.
2. Caselles, V., Kimmel, R., and Sapiro, G., Geodesic active contours, *Int. J. Comput. Vision*, 1997, vol. 22, pp. 61–79.
3. Paragios, N. and Deriche, R., Geodesic active contours and level sets for detection and tracking of moving objects, *IEEE Trans. Pattern Anal. Mach. Intell.*, 2000, vol. 22, pp. 1–15.
4. Vasilevskiy, A. and Siddiqi, K., Flux-maximizing geometric flows, *IEEE Trans. Pattern Anal. Mach. Intell.*, 2000, vol. 24, pp. 1565–1578.
5. Li, C., Xu, C., Gui., and Fox, M.D., Level set evolution without re-initialization: a new variational formulation, in: *IEEE Conf. Comput. Vision Pattern Recognit.*, San Diego, 2005.
6. Zhu, G., Zhang, S., Zeng, Q., and Wang, C., *Boundary-based image segmentation using binary level set method*, *SPIE OE Lett.*, 2007, vol. 46.
7. Chan, T.F. and Vese, L.A., Active contour without edges, *IEEE Trans. Image Process.*, 2000, vol. 10, pp. 266–277.
8. Ronfard, R., Region-based strategies for active contour models, *Int. J. Comput. Vision*, 2002, vol. 46, pp. 223–247.
9. Lie, J., Lysaker, M., and Tai, X.C., *A binary level set model and some application to Mumford-Shah image segmentation, IEEE Trans. Image Process.*, 2006, vol. 15, pp. 1171–1181.
10. Tsai, A., Yezzi, A., and Willsky, A.S., Curve evolution implementation of the Mumford-Shah functional for image segmentation, denoising, interpolation, and magnification, *IEEE Trans. Image Process.*, 2001, vol. 10, pp. 1169–1186.
11. Vese, L.A. and Chan, T.F., A multiphase level set framework for image segmentation using the Mumford-Shah model, *Int. J. Comput. Vision*, 2002, vol. 50, pp. 271–29.
12. Liu, H., Chen, Y., Chen, Y., and Chen, W., Neighborhood aided implicit active contours, *IEEE Conf. Comp. Vision Pattern Recognit.*, 2006, pp. 841–848.
13. Wang, Z. and Vemuri, B.C., Tensor field segmentation using region based active contour model, *Proc. Eighth Eur. Conf. Comput. Vision (ECCV'04)*, Springer Lecture, 2004, pp. 304–315.

14. Mumford, D. and Shah, J., Optimal approximation by piecewise smooth function and associated variational problems, *Comm. Pure Appl. Math*., 1989, vol. 42, pp. 577–685.
15. Wang, L., He, L., Mishra, A., and Li, C., Active contours driven by local Gaussian distribution fitting energy, *Sci. Direct Signal Process*., 2009, vol. 89, pp. 2435–2447.
16. Li, C., Kao, C., Gore, J., and Ding, Z., Minimization of region-scalable fitting energy for image segmentation, *IEEE Trans. Image Process*., 2008, vol. 17, pp. 1940–1949.
17. Li, C., Kao, C., Gore, J., and Ding, Z., Implicit active contour driven by local binary fitting energy, *Proc. IEEE Conf. Comput. Vision Pattern Recognit. (CVPR)*, 2007, pp. 1–7.
18. Wang, Y. and He, C., Image segmentation algorithm by piecewise smooth approximation, *EURASIP J. Image Video Process*., 2012, pp. 1687–5281.
19. Zhang, H.S.K. and Zhang, L., Active contours driven by local image fitting energy, *Pattern Recognit*., 2010, vol. 43, pp. 1199–1206.
20. Wang, X.F., Huang, D., and Xu, H., An efficient local Chan-Vese model for image segmentation, *Pattern Recognit*., 2010, vol. 43, pp. 603–618.
21. Wang, H., Huang, T.Z., Xu, Z., and Wang, Y., An active contour model and its algorithms with local and global Gaussian distribution fitting energies, *Inf. Sci*., 2014, vol. 263, pp. 43–59.
22. Osher, S. and Sethian, J.A., Front propagating with curvature dependent speed: algorithm based on Hamilton-Jacobi formulations, *J. Comput. Phys*., 1988, vol. 79, pp. 12–49.
23. Aubert, G. and Kornprobst, P., Mathematical problems in image processing partial differential equations and the calculus of variations, *Appl. Math. Sci*., p. 147.
24. Nacereddine, N., Tridi, M., Hamami, L., and Ziou, D., Statistical tools for weld defect evaluation in radiographic testing, *J. Nondestr. Test. Ultrason. ECNDT*, 2006, pp. 1–21.
25. Al-Najjar, Y.A.Y. and Soong, D.C., Comparison of image quality assessment: PSNR, HVS, SSIM, UIQI, *Int. J. Sci. Eng. Res*., 2012, pp. 1–5.
26. Wang, Z. and Bovik, A., A universal image quality index, *IEEE Signal Process. Lett*., 2002, vol. 9, p. 81.